

Direct Observation of Conductive Polymer Induced Inversion Layer in n-Si and Correlation to Solar Cell Performance

Rongbin Wang, Yusheng Wang, Chen Wu, Tianshu Zhai, Jiacheng Yang, Baoquan Sun,*
Steffen Duhm,* and Norbert Koch*

Heterojunctions formed by ultrathin conductive polymer [poly(3,4-ethylenedioxythiophene): poly(styrenesulfonate)—PEDOT:PSS] films and n-type crystalline silicon are investigated by photoelectron spectroscopy. Large shifts of Si 2p core levels upon PEDOT:PSS deposition provide evidence that a dopant-free p–n junction, i.e., an inversion layer, is formed within Si. Among the investigated PEDOT:PSS formulations, the largest induced band bending within Si (0.71 eV) is found for PH1000 (high PEDOT content) combined with a wetting agent and the solvent additive dimethyl sulfoxide (DMSO). Without DMSO, the induced band bending is reduced, as is also the case with a PEDOT:PSS formulation with higher PSS content. The interfacial energy level alignment correlates well with the characteristics of PEDOT:PSS/n-Si solar cells, where high polymer conductivity and sufficient Si-passivation are also required to achieve high power conversion efficiency.

hene):poly(styrenesulfonate) (PEDOT:PSS) as one of the electrical contacts have drawn wide attention in the recent years due to the low-temperature and cost-effective deposition process of PEDOT:PSS, while at the same time retaining the potential for high power conversion efficiency (PCE).^[1] In a typical Al/n-Si/PEDOT:PSS/Ag grid solar cell, light illumination generates electron–hole pairs in Si. The holes are then transported by the PEDOT:PSS layer to the Ag electrode and the electrons are collected at the Al electrode.^[2] The most pivotal part of such a solar cell is the PEDOT:PSS layer, which was suggested to fulfill four main tasks:^[3] i) it induces an inversion layer in n-Si (i.e., a p-dopant-free Si p–n junction is formed) to block electrons and extract

1. Introduction

Heterojunction solar cells utilizing n-type crystalline Si (n-Si) as absorber and the conducting polymer poly(3,4-ethylenedioxythiophene):poly(styrenesulfonate) (PEDOT:PSS) as one of the electrical contacts have drawn wide attention in the recent years due to the low-temperature and cost-effective deposition process of PEDOT:PSS, while at the same time retaining the potential for high power conversion efficiency (PCE).^[1] In a typical Al/n-Si/PEDOT:PSS/Ag grid solar cell, light illumination generates electron–hole pairs in Si. The holes are then transported by the PEDOT:PSS layer to the Ag electrode and the electrons are collected at the Al electrode.^[2] The most pivotal part of such a solar cell is the PEDOT:PSS layer, which was suggested to fulfill four main tasks:^[3] i) it induces an inversion layer in n-Si (i.e., a p-dopant-free Si p–n junction is formed) to block electrons and extract

holes, ii) it transports holes to the metal anode, iii) it acts as a surface passivation layer to reduce interfacial recombination, and iv) it increases light harvesting by reducing reflection. Therefore, appropriate PEDOT:PSS/Si interface formation and properties are key to achieve high-performance solar cells.^[2b,3,4] However, despite numerous attempts, such as improving the conductivity of the PEDOT:PSS layer,^[5] using nanostructured Si surfaces,^[1b,4a] deposition of interlayers,^[6] and others,^[7] the PCE achieved with dopant-free approaches for Si-based solar cells has still room for improvement.^[8]

The properties of PEDOT:PSS thin films are well investigated and are mostly in line with the above mentioned tasks ii–iv).^[1d,9] However, evidencing and quantifying the effectiveness of task i) is not straightforward. The work function (WF) of commonly used PEDOT:PSS formulations spreads from ≈ 4.65 to 5.20 eV^[10] and is thus—assuming Schottky-contact formation—not high enough to induce a strong inversion layer in n-Si.^[11] The surface chemical composition of PEDOT:PSS on n-Si with or without solvent treatment^[2b,5b,12] as well as indirectly assessed energy level alignment^[7c,13] have been reported. However, direct evidence for the most fundamental interfacial property, i.e., the inversion layer formation, is still missing. The inversion layer has so far been assumed based on capacitance–voltage measurements or by comparing the WF differences between PEDOT:PSS and n-Si, without using the information on band bending potentially contained in core level (Si 2p) shifts as obtained in X-ray photoelectron spectroscopy (XPS).^[7b,13b,14] On the other hand, for a functionally related interface, i.e.,

R. Wang, Y. Wang, C. Wu, T. Zhai, J. Yang, Prof. B. Sun, Prof. S. Duhm, Prof. N. Koch

Institute of Functional Nano and Soft Materials (FUNSOM)
Joint International Research Laboratory of Carbon-Based Functional
Materials and Devices and Jiangsu Key Laboratory for Carbon-Based
Functional Materials and Devices

Soochow University

215123 Suzhou, P. R. China

E-mail: bqsun@suda.edu.cn; duhm@suda.edu.cn;

norbert.koch@physik.hu-berlin.de

R. Wang, Prof. N. Koch

Institut für Physik und IRIS Adlershof


Humboldt-Universität zu Berlin

Brook-Taylor-Str. 6, 12489 Berlin, Germany

Prof. N. Koch

Helmholtz-Zentrum Berlin für Materialien und Energie GmbH

Albert-Einstein Str. 15, 12489 Berlin, Germany

 The ORCID identification number(s) for the author(s) of this article can be found under <https://doi.org/10.1002/adfm.201903440>.

© 2019 The Authors. Published by WILEY-VCH Verlag GmbH & Co. KGaA, Weinheim. This is an open access article under the terms of the Creative Commons Attribution License, which permits use, distribution and reproduction in any medium, provided the original work is properly cited.

DOI: 10.1002/adfm.201903440

MoO_x/n-Si, the existence of an inversion layer was evidenced by the shift of Si core level upon incremental deposition of MoO_x^[15] and the observed strong inversion could be explained by the huge WF (around 6.90 eV)^[16] of MoO_x.^[11] Such incremental deposition from the sub-nm to the several ten-nm film thickness is not readily practical for PEDOT:PSS as it is deposited from aqueous dispersion, often leading to inhomogeneous films and pinholes in the ultrathin film regime. Therefore, only few reports addressed Si core-level evolution,^[6b,17] which could provide the desired information to more directly assess band bending within the inorganic semiconductor.

The challenge to measure the Si core level with XPS is related to the PEDOT:PSS layer thickness, which is usually larger than 30 nm,^[17a] and thus beyond the photoelectron mean-free path (much less than 10 nm) when employing typical lab-based setups.^[18] One possible workaround is using hard X-ray photoelectron spectroscopy (HAXPES), which increases the mean-free path of photoelectrons due to a much higher excitation photon energy.^[19] For instance, Jäckle et al. utilized HAXPES to probe the buried n-Si/PEDOT:PSS interface by removing excess PSS on the top surface, yet thereby altering the surface properties.^[17a] An alternative is to directly prepare a thinner layer of PEDOT:PSS, i.e., less than 10 nm, despite the challenge named above. When spin coating polymers from solution in a well-controlled manner, ultrathin layers can be obtained by decreasing the solution concentration while increasing the spin coating speed.^[17b,20]

In the present work, we mimicked incremental deposition of PEDOT:PSS on n-Si by adjusting the solution concentration and spin speed. We obtained a series of homogeneous and continuous PEDOT:PSS films with thickness ranging from 5 to 50 nm (as determined by ellipsometry) on the n-Si surface. The electronic properties of these interfaces were investigated by ultraviolet photoelectron spectroscopy (UPS) and XPS. Based on the direct observation of Si 2p core level shifts, we found that PEDOT:PSS indeed induces substantial band bending in n-Si, leading to an inversion layer. In addition, we show that the solvent additive dimethyl sulfoxide (DMSO) boosts the band bending in Si in addition to conductivity enhancement.^[9e] We also compare the interface properties formed by PEDOT:PSS with different PEDOT to PSS ratio, and provide reliable energy level diagrams for these heterojunctions. In model solar cells, a higher PEDOT concentration as well as the addition of DMSO resulted in improved device performance due to a higher open-circuit voltage (V_{oc}) and higher conductivity through the polymer layer. The clear-cut relations between interface electronic properties, transport through PEDOT:PSS, and solar cell function provide a solid base for further pushing the development and performance of dopant-free heterojunctions in electronic and optoelectronic devices.

2. Results

We first discuss the XPS results obtained for the high-conductivity formulation PH1000 (PEDOT:PSS mass ratio of 1:2.5),^[9e,21] deposited on n-Si from solution with Triton X-100 (hereafter referred to as Triton) and DMSO additives. The Si 2p_{3/2} peak of the reference sample (pristine HF-treated n-Si) is centered at 99.89 eV (Figure 1a) and can be ascribed to Si–Si bonds,^[6b,22]

with no detectable SiO_x species at higher binding energy (BE). For the 5 nm thick PEDOT:PSS layer, the Si 2p_{3/2} peak is centered at 99.27 eV BE, much lower in energy than that of pristine n-Si. A weak higher BE Si 2p signal (ca. 102–103 eV) can be ascribed to various Si–O bonds,^[23] indicating the presence of SiO_x on the Si surface, yet much thinner than the native oxide (see below). For thicker PEDOT:PSS films (7–12 nm), the Si 2p main peak shifts to even lower BE and the intensity of the SiO_x-derived peak slightly increases (Table S1, see Supporting Information). The Si 2p_{3/2} peak is centered at 99.18 eV BE for the 12 nm thick PEDOT:PSS film, giving an energy difference of 0.71 eV with respect to the pristine n-Si. The shift might further increase slightly for higher PEDOT:PSS thickness, but the intensity of the Si 2p peak was then too small to be detected. However, the vast majority of the shift occurs for the 5 nm thick polymer film (0.62 eV), and up to 12 nm thick PEDOT:PSS only an additional 0.09 eV occurs. Qualitatively similar Si 2p core level shifts, indicative of surface band bending in n-Si, were reported for coating Si with other polymers^[24] or with small organic molecules.^[17b,25] The S 2p core level spectra (Figure 1b) show two major contributions, one from PSS at the high BE side and the other from PEDOT at the low BE side.^[10a,26] Since some of the sulfonate units of PSS gain electrons from PEDOT, charged and neutral species (PSS[−] and PSSH)^[27] contribute to the S 2p core levels. The positive charges are delocalized over the PEDOT chains, resulting in a broad asymmetric tail on the high BE side of the PEDOT S 2p peaks.^[27,28] With increasing nominal PEDOT:PSS thickness, the atomic ratio of S 2p to Si 2p increases (Table 1, and Figure S1, Supporting Information), which confirms the ellipsometry data.

Figure 2 shows the UPS spectra of samples S1–S4, whose core levels are discussed above (and shown in Figure 1). The WF of pristine n-Si is 4.18 eV, and after deposition of PEDOT:PSS it increases to 4.58–4.66 eV, essentially independent of PEDOT:PSS thickness. This implies that even such ultrathin PEDOT:PSS films already exhibit the WF of thick films, which can be understood from the fact that the WF of PEDOT:PSS is determined by both the bulk electrochemical potential of electrons inside the film and the surface dipole, which is formed by the surface enrichment of negatively charged PSS compared to positively charged PEDOT.^[10a] The remaining small variation for the present samples can be ascribed to the small fluctuation of the ratio between PEDOT and PSS on the surface.^[29] The ratio of PSS and PEDOT in each film was determined by the atomic ratio of its respective S 2p peaks, as given in Table 1. The valence band region near the Fermi level of all four layers shows no noticeable changes and the density of valence band states is virtually identical, in line with the almost constant WF.

In the following, we turn towards the photoemission characterization of PEDOT:PSS films obtained with/without additives and also from a different formulation. Figure 3 shows the Si 2p and S 2p core level spectra obtained from 12 nm thick PEDOT:PSS (PH1000+Triton) with and without DMSO, as well as a 12 nm thick PEDOT:PSS (Al4083+Triton) with DMSO, respectively. The spectra of pristine n-Si and, for comparison, 1.6 nm thick MoO_x on n-Si serve as reference for the discussion. Compared with the Si 2p_{3/2} peak of pristine n-Si, the largest shift occurs for the 1.6 nm thick MoO_x layer ($\Delta_{Si2p} = 0.83$ eV), and the second largest shift ($\Delta_{Si2p} = 0.71$ eV) occurs for the already discussed 12 nm thick PEDOT:PSS

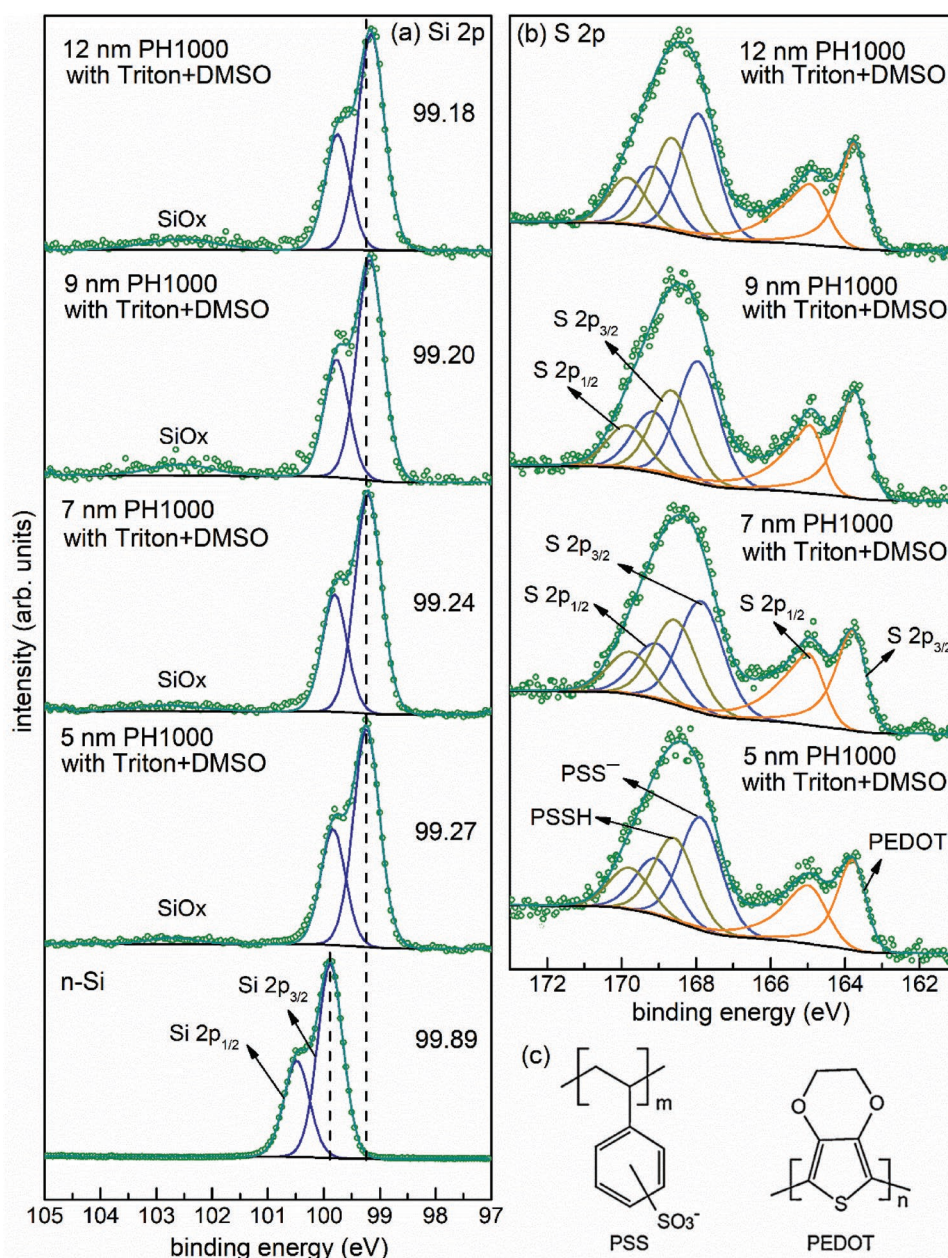


Figure 1. XPS spectra of a) Si 2p and b) S 2p core levels from n-Si and PEDOT:PSS layers (PH1000 + 1 wt% Triton + 5 wt% DMSO) with different thickness (as indicated in each plot; corresponding to samples S1–S4 from Table 4). c) Chemical structure of PEDOT and PSS.

(PH1000+Triton) with DMSO. Without DMSO, the smallest shift ($\Delta_{\text{Si}2p} = 0.30$ eV) in this series is observed. For the other formulation of PEDOT:PSS (Al4083+Triton) with DMSO, $\Delta_{\text{Si}2p}$ is 0.57 eV. Besides that, for all PEDOT:PSS thin films, a weak SiO_x signal appears, which, e.g., has also been found upon deposition of TiO_x^[30] or 3-glycidioxy-propyltrimethoxysilane^[6b] on Si. This ultrathin SiO_x can act as surface passivation layer to suppress charge recombination. For the 1.6 nm thick MoO_x film, on the other hand, no SiO_x signal was detected. This can be explained by the comparably high density of oxygen vacancies typically found in sublimed MoO_x layers, so the n-Si surface does not form bonds with the oxygen in MoO_x.^[15]

The atomic ratios of S/Si (Table 1) of the 12 nm thick PEDOT:PSS films with and without DMSO are 2.40 and 1.21, respectively. This demonstrates that DMSO indeed improves the film coverage and homogeneity^[9e] and decreases the fraction of uncovered or barely covered Si after spin-coating. As for the ratio of PSS and PEDOT, the PEDOT:PSS films without DMSO have a higher PSS surface content compared to those with DMSO. The films made from Al4083 have significantly less PEDOT, as expected from the specified mass ratio between PSS and PEDOT for Al4083 of 6.0, whereas it is only 2.5 for PH1000.

The PSS/PEDOT ratio variation also influences the valence electron features close to the Fermi level (Figure 4). In general,

Table 1. Detailed information for all films and substrates based on XPS and UPS results.

Samples	Thickness [nm]	BE of Si 2p _{3/2} (Si—Si bond) [eV]	Atomic ratio of S(PSS)/S(PEDOT)	Atomic ratio of S(S2p) /Si(Si2p)	WF [eV]	Δ_{BE} with respect to n-Si Si 2p _{3/2} [eV]	Δ_{WF} with respect to n-Si [eV]
n-Si	—	99.89	—	—	4.18	—	—
S1 PH1000 Triton+DMSO/n-Si	5	99.27	2.36	1.23	4.58	0.62	0.40
S2 PH1000 Triton+DMSO/n-Si	7	99.24	2.38	1.41	4.59	0.65	0.41
S3 PH1000 Triton+DMSO/n-Si	9	99.20	2.50	2.26	4.63	0.69	0.45
S4 PH1000 Triton+DMSO/n-Si	12	99.18	2.48	2.40	4.66	0.71	0.48
S5 PH1000 Triton+DMSO/n-Si	50	—	2.37	—	4.70	—	0.52
S6 PH1000 Triton/n-Si	12	99.59	2.78	1.21	4.49	0.30	0.31
S7 PH1000 Triton/n-Si	50	—	3.00	—	4.80	—	0.62
S8 Al4083 Triton+DMSO/n-Si	12	99.32	5.98	4.99	4.66	0.57	0.48
S9 Al4083 Triton+DMSO/n-Si	50	—	6.01	—	4.83	—	0.65
SiO ₂ (Si with a native oxide layer)	—	99.64	—	—	4.43	0.25	0.25
S10 PH1000/SiO ₂	12	99.29	2.71	5.70	4.90	0.60 (0.35) ^{a)}	0.72 (0.48) ^{a)}

^{a)}With SiO₂ substrate as reference.

the intensity of these features increases with increasing PEDOT concentration near the surface. In particular, the Al4083 films with a PSS/PEDOT ratio of ≈ 6 (Table 1) exhibit the lowest intensity. For the PH1000 films, the addition of DMSO decreases the PSS/PEDOT ratio only slightly from ≈ 3 to ≈ 2.5 , but the intensity of the valence features is increased substantially. A similar observation was made for another additive, diethylene glycol, to the PEDOT:PSS solution.^[31] For all three different PEDOT:PSS film types discussed here, the thickness has almost no impact on the valence electron features. However, for the two PH1000 films without DMSO, the WF values are 4.49 and 4.80 eV for the 12 and the 50 nm

thick films, respectively. This difference may have further causes in addition to the difference of the PSS/PEDOT ratio. The WF of PEDOT:PSS films can be also affected by annealing temperature, residual water content, or solvent treatment.^[10,29,32] Without DMSO, a coiled conformation of PEDOT:PSS cores surround by excess PSS shells prevails,^[9e] likely resulting in incomplete Si coverage, which could also account for the lower WF of the 12 nm film.^[33]

To exclude effects induced by the wetting agent Triton and the co-solvent DMSO on the band bending in Si, hydrophilic SiO₂^[34] was used as substrate for PH1000 without Triton and DMSO. The Si 2p core level peaks are shown in Figure 5 and the main parameters are summarized in Table 2. For the PEDOT:PSS film on SiO₂, the shift of the elemental Si peak is 0.35 eV compared to bare SiO₂. In contrast, the SiO_x related peak shifts by 0.58 eV. This non-rigid shift implies that, in addition to inducing band bending in Si, PEDOT:PSS also further oxidizes the substrate, which is corroborated by the intensity increase of the SiO_x related peak upon PEDOT:PSS deposition. It can be thus inferred that PEDOT:PSS itself (and not Triton) induces also the majority of the band bending of the HF-treated n-Si and generates the interfacial SiO_x species on top. However, it still remains to be clarified whether simply the water of the solution induces the SiO_x formation, or whether other components also form Si—O bonds at the surface. Therefore, in several reference experiments, PSS, Triton, and DMSO as well as combinations of these were deposited on n-Si substrates, the corresponding Si 2p core levels spectra are shown in Figure S2 in the Supporting Information. From all these samples, only PSS alone did not induce detectable SiO_x species. The wetting agent Triton induced the highest SiO_x amount. Possibly, PEDOT could also form Si—O bonds since the positively charged PEDOT could receive electrons from Si and bind to the surface.

Based on the photoelectron spectroscopy results, we used three different PEDOT:PSS film types to fabricate Al/Si/PEDOT:PSS/Ag solar cells: PH1000+Triton,

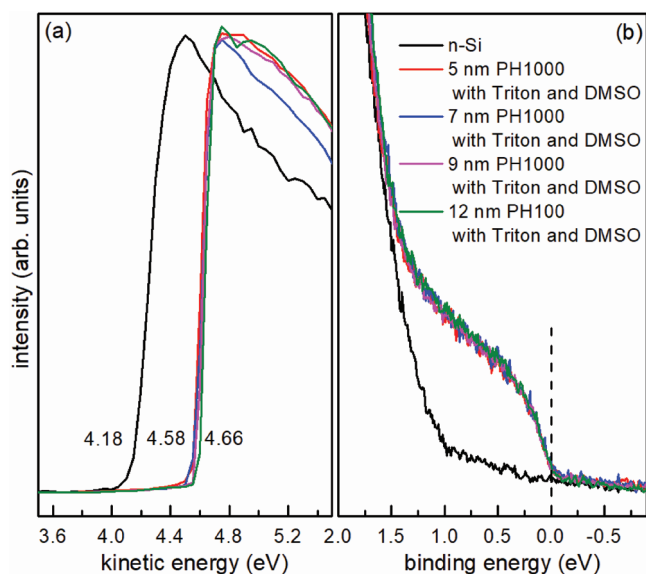


Figure 2. UPS spectra of a) secondary electron cut-off (SECO) and b) valence band region near the Fermi level (set to zero) for n-Si without and with PEDOT:PSS layers (PH1000 + 1 wt% Triton + 5 wt% DMSO) of different thickness (as indicated in the plot).

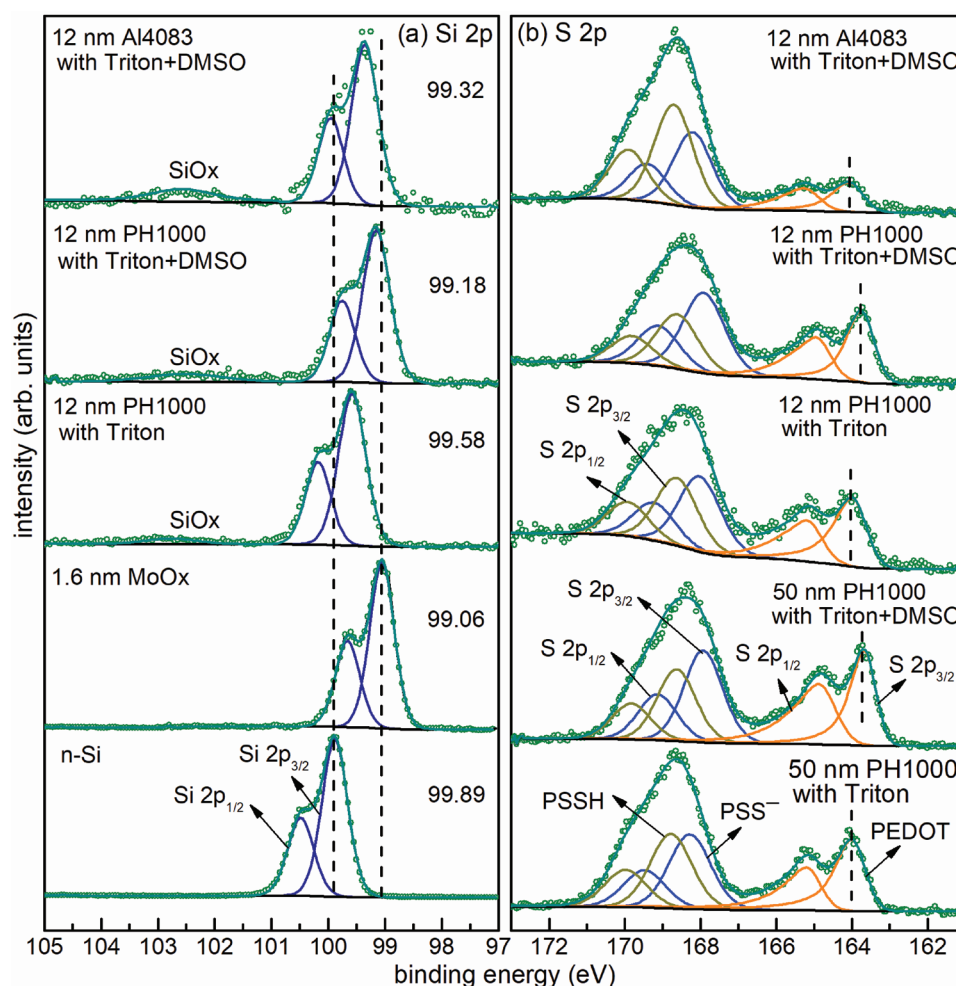


Figure 3. a) XPS spectra of Si 2p core levels obtained from bare n-Si, and coated with 1.6 nm MoO_x, 12 nm PEDOT:PSS (PH1000+Triton) with and without DMSO, and 12 nm PEDOT:PSS (Al4083+Triton) with DMSO. b) XPS spectra of S 2p core levels obtained from 12 and 50 nm PEDOT:PSS (PH1000+Triton) with or without DMSO, and 12 nm PEDOT:PSS (Al4083+Triton) with DMSO, on n-Si.

PH1000+Triton+DMSO, and Al4083+Triton+DMSO. The current density–voltage curves and the electrical output characteristics of these, and of an Al/Si/MoO_x/Ag reference device, are shown in **Figure 6** and summarized in **Table 3**. From all four devices, the solar cell with PH1000+Triton+DMSO shows the highest PCE. That of the MoO_x reference device is less than half, which is, as the open circuit voltage (V_{oc}) is only slightly decreased, mainly due to the significantly lower short circuit current (J_{sc}) and fill factor (FF). Although the MoO_x layer does induce the desirable band bending in n-Si (≈ 0.80 eV^[15] and this work), the low conductivity and inferior interfacial passivation properties not only decrease the hole extraction and transport efficiency, but also increase the recombination rate at the interface.^[3] For the PH1000 device without DMSO, the PCE is further decreased, which is mainly due to a rather low J_{sc} , consistent with previous data.^[2b] The solar cell with Al4083 has the lowest PCE of all devices, as well as the lowest V_{oc} .

The highest PCE found in the present work is 10.23% with $V_{oc} = 0.64$ V, $J_{sc} = 23.01$ mA cm⁻², and FF = 0.70, which is comparable to other reported planar solar cell types in the ‘front-PEDOT:PSS/Si’ architecture.^[35] As the planar architecture

suffers from significant reflection losses, a textured or hierarchical structure can be introduced on the front side of Si to avoid it, enabling reaching a higher PCE of 17%–18% with $V_{oc} = 0.61$ – 0.64 V, $J_{sc} = 37.5$ – 38.4 mA cm⁻², and FF = 0.74–0.76.^[35,36] Moreover, to avert the absorption caused by PEDOT:PSS layer, a ‘back-PEDOT:PSS/Si’ architecture can be implemented by depositing PEDOT:PSS on the back side of Si. In such a way, the PCE can reach $\approx 20\%$ for p-type Si^[37] and 21% for n-type Si,^[38] both with a textured Si surface on the front side.

3. Discussion

The results of our XPS and UPS studies are summarized in the energy level diagrams in **Figure 7**. For the 12 nm thick PH1000+Triton film (**Figure 7a**), the energy shift of the Si 2p core level ($\Delta E = 0.30$ eV) is almost the same as the WF difference between n-Si and the PEDOT:PSS layer ($\Delta W_F = 0.31$ eV), which appears to be in line with Schottky-contact formation.^[39] For the 50 nm thick film (**Figure 7d**), it is not possible to measure the Si 2p signal with XPS due to the

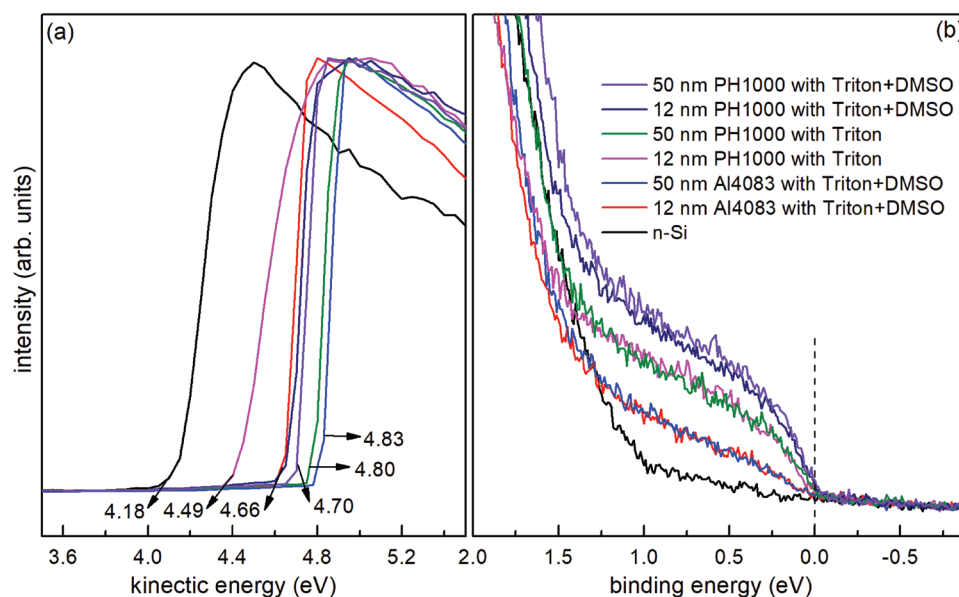


Figure 4. UPS spectra of a) SECO and b) valence band region near the Fermi level.

thick overlayer, thus only a lower limit of the band bending is shown in the Si side. However, it could be that the band bending magnitude is the same as Δ_{WF} (0.62 eV). For several other of the interfaces, Δ_{BE} is in fact larger than Δ_{WF} , i.e., the band bending magnitude exceeds the difference between the WF of the respective material surfaces. This happens in particular for the 12 nm PH1000+Triton+DMSO film (Figure 7b) and the 12 nm Al4083+Triton+DMSO film (Figure 7c), which do not follow the simple Schottky-contact model.^[15,39,40] As

noted in the Introduction, the PEDOT:PSS films cannot be constructed layer by layer to assess more details of the very interface to n-Si. Nevertheless, based on our data, we propose two possible scenarios for the buried interface. We use the 50 nm PH1000+Triton+DMSO film (Figure 7e), which shows the best performance in the device, as the model system. The lower limit of the band bending magnitude is 0.71 eV and Δ_{WF} is 0.52 eV. The difference of 0.19 eV can either be due to a drop of the electrostatic potential i) at the Si–PEDOT:PSS interface, or ii) at the surface (facing vacuum) of the PEDOT:PSS film (compare schematic energy level diagrams in Figure S3, Supporting Information). Given the complex process of PEDOT:PSS film formation, it is plausible that (on average) the vertical distribution of PEDOT versus PSS differs at the bottom (interface to Si) and top of the film. Since the WF of PEDOT:PSS is significantly impacted by the surface dipole (PSS-enrichment at the surface increases the WF; see above), it could thus well be that this dipole is different at the bottom compared to the top surface, thus yielding different local electrostatic potentials, as indicated in Figure 7. However, the evolution of the potential energy within the PEDOT:PSS layer does not play a crucial role for device performance, as potential variations do not impact charge transport in the valence levels.

Our XPS data evidence that PEDOT:PSS can induce band bending within n-Si for both, bare and native oxide covered surfaces. For the magnitude of the band bending, two main aspects play important roles: the formulation of PEDOT:PSS and whether DMSO is added or not. The first aspect determines the relative amount of PEDOT that is available close to the n-Si. For PH1000 and Al4083, the mass ratio between PEDOT and PSS is 1:2.5 and 1:6, respectively. As shown in Figure 7, the 12 nm thick PH1000 film (with Triton and DMSO) induces a larger band bending magnitude than the 12 nm thick Al4083 film. The second aspect pertains to how the PEDOT:PSS makes contact with n-Si nanoscopic in detail. Many reports have shown that by adding DMSO into the original PEDOT:PSS aqueous

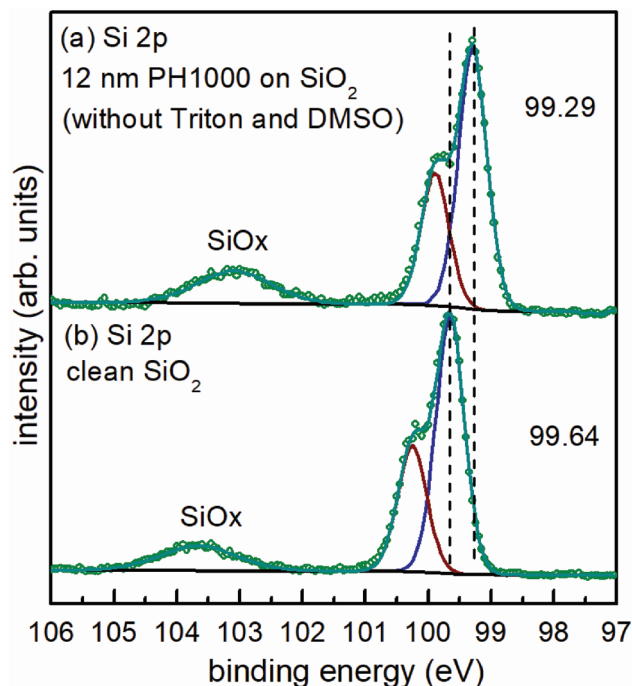


Figure 5. XPS spectra of Si 2p for a) 12 nm PEDOT:PSS (PH1000, without Triton and DMSO) on SiO_2 , and b) bare SiO_2 .

Table 2. Comparison of bare SiO₂ and 12 nm PEDOT:PSS (PH1000 without Triton and DMSO) film on SiO₂.

Substrate	BE of Si 2p _{3/2} (Si–Si bond) [eV]	BE of Si 2p (Si–O bond) [eV]	Work function [eV]	Δ_{BE} between Si 2p _{3/2} (Si–Si) and Si 2p (Si–O) [eV]	Atomic ratio between Si (Si–O) and Si (Si–Si)
SiO ₂	99.64	103.66	4.42	4.02	0.17
12-nm-thick PH1000 on SiO ₂	99.29	103.08	4.93	3.79	0.23
Δ	0.35	0.58	–0.51	0.23	–0.06

solution, after annealing films feature a thinner outside PSS-rich-shell and coiled PEDOT-rich cores, compared to the case without DMSO, which also improves the conductivity of the film by reducing the width of insulating PSS shells.^[2b,9e,17a,21b] The thinner PSS-rich shell also enhances the direct contact possibility between PEDOT and Si. Then more electrons can transfer from n-Si to PEDOT (or coiled PEDOT:PSS), leading to a larger band bending. Indeed, by comparing the two 12 nm PEDOT:PSS (PH1000) films with and without DMSO, it becomes apparent that adding DMSO more than doubles the band bending magnitude.

The photoelectron spectroscopy data also allow explaining the solar cell data. In particular, the V_{oc} is related to the band bending magnitude,^[24] and J_{sc} and FF to the density of states close to E_F .^[41] The PH1000+Triton+DMSO film, which induces the largest band bending magnitude (Figure 1) and the largest density of states close to E_F (Figure 4), enables also the largest V_{oc} , J_{sc} , FF, and, consequently, PCE (Table 3). For Al4083+Triton+DMSO, XPS indicates that the band bending is only 0.57 eV (Figure 3) and UPS unravels a comparably low density of states (Figure 4); as a result, the V_{oc} and mainly J_{sc} and FF are largely decreased. A paradox seems to appear for PH1000+Triton as the qV_{oc} (0.62 eV) of the device is larger than the induced band bending (0.30 eV) obtained by XPS. Most likely, with increasing thickness of the PEDOT:PSS layer, a yet improved interface is formed, which induces a larger band bending compared with that of the low coverage of 12 nm film. Intriguingly, the J_{sc} of the three PEDOT:PSS/Si devices do follow the intensity of the density of valence states, supporting

that indeed the density of states correlates with the conductivity of the PEDOT:PSS film.

Overall, our results show that a small induced band bending will lead to a small V_{oc} , however, large band bending does not always result in a high V_{oc} . The hole extraction and transport efficiencies of the layer inducing the band bending in Si also need to be taken into account. In a heterojunction silicon solar cell, the layer itself and its interface with the silicon are key aspects in determining the device performance.^[1a,5b,30] The optimization of the device should follow the discussed two points: first, a sufficiently large induced band bending in Si is required in order to achieve efficient hole extraction and prevent the transport of electrons to the anode;^[7a,15] second, this layer should also have adequate conductivity to transport the holes to the anode and simultaneously reduce the recombination rate at the interface.^[1b,3]

4. Conclusion

We directly evidenced that PEDOT:PSS induces a large upward band bending in n-Si, even reaching inversion conditions. By diluting the original PEDOT:PSS solution and increasing the spin-coating speed, a series of PEDOT:PSS thin films with nominal thicknesses down to 5 nm were achieved on n-Si substrates. Polymer-induced band bending and inversion layer formation within Si were revealed by shifts of the Si 2p core levels. We found that adding DMSO to the polymer solution or increasing the PEDOT to PSS ratio increase the band bending magnitude. Moreover, the addition of DMSO improves the interface between PEDOT:PSS and n-Si, as reflected by the performance of PEDOT:PSS/n-Si solar cells, and the formulation PH1000 with DMSO yielded the largest V_{oc} (0.64 V), which is comparable with that of classical Si solar cell. By comparing PEDOT:PSS/n-Si solar cells with MoO_x/n-Si cells, it becomes apparent that a large contact-induced band bending does not necessarily lead to a high V_{oc} . Adequate passivation of the silicon surface to decrease recombination and high conductivity of the polymer layer are also needed to achieve high PCE devices. Further optimization of PEDOT:PSS/n-Si solar cells should pursue an improved interface between PEDOT:PSS and n-Si, e.g., by increasing the PEDOT concentration and molecular passivation of the Si.

5. Experimental Section

Sample Preparation: Coupons cut from n-type (100)-oriented, single-side polished and 300 μm thick single crystal Si wafers (0.05–0.1 $\Omega\text{ cm}$, Resemi semiconductor Co. Ltd) with a native oxide layer were used for all samples. The coupons were ultrasonically

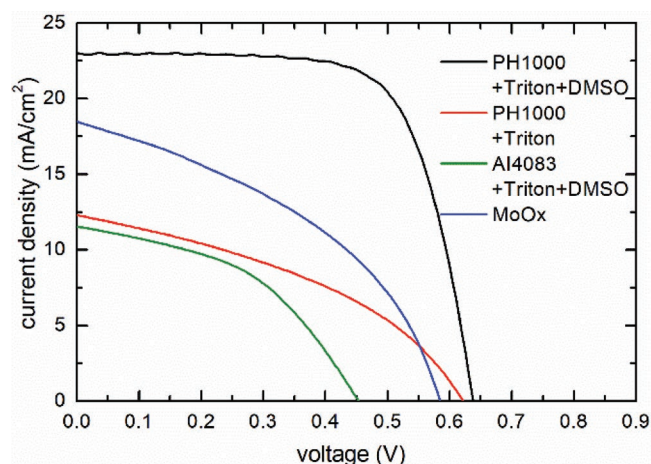


Figure 6. J – V curves under AM 1.5 illumination of 100 mW cm^{-2} of Al/Si/PEDOT:PSS (PH1000+Triton+DMSO)/Ag, Al/Si/PEDOT:PSS (PH1000+Triton)/Ag, Al/Si/PEDOT:PSS (Al4083+Triton+DMSO)/Ag and Al/Si/MoO_x/Ag silicon-based solar cells.

Table 3. Electrical characteristics of the solar cells, and band bending magnitude and density of PEDOT:PSS valence states obtained from UPS.

Device	V_{oc} [V]	J_{sc} [mA cm^{-2}]	FF	PCE [%]	Band bending [eV]	Valence state density
Al/Si/MoO _x /Ag	0.58	18.49	0.42	4.45	0.80	–
Al/Si/PEDOT:PSS (PH1000+Triton)/Ag	0.62	12.29	0.40	3.03	0.30	Medium
Al/Si/PEDOT:PSS (PH1000+Triton+DMSO)/Ag	0.64	23.01	0.70	10.23	0.71	High
Al/Si/PEDOT:PSS (Al4083+Triton+DMSO)/Ag	0.45	11.54	0.45	2.34	0.57	Low

cleaned in acetone, ethanol, and deionized (DI) water, followed by UV-ozone treatment for 15 min. Subsequently, they were immersed in HF solution for 5 min to remove the native oxide layer and then washed with DI water, before measurements or polymer coating. Two different PEDOT:PSS formulations were used: PH1000 (Clevios) with a PEDOT:PSS mass ratio of 1:2.5 and Al4083 (Clevios) with a mass ratio of 1:6. After removal of the Si oxide layer the surface becomes hydrophobic due to the H-termination, and it is necessary to add Triton X-100 (Alfa Aesar) as wetting agent into the PEDOT:PSS aqueous solution to ensure proper thin film formation on Si. After

spin-coating of PEDOT:PSS, samples were annealed for 20 min at 125 °C. Film thickness determination was carried out by spectroscopic ellipsometer (J. A. Woollam Corporation, Alpha-SE). Details of all samples are given in **Table 4**. For each sample type, at least two individual samples were investigated to warrant reproducibility. For select cases, up to five samples were investigated. The electrical conductivity of PH1000 (1 wt% Triton and 5 wt% DMSO), PH1000 (1 wt% Triton), and Al4083 (1 wt% Triton and 5 wt% DMSO) thin films (≈ 60 nm) coated on glass was determined to be $500 (\pm 15)$, $84 (\pm 12)$, and $< 0.1 \text{ S cm}^{-1}$, respectively, by the four-point probe method.

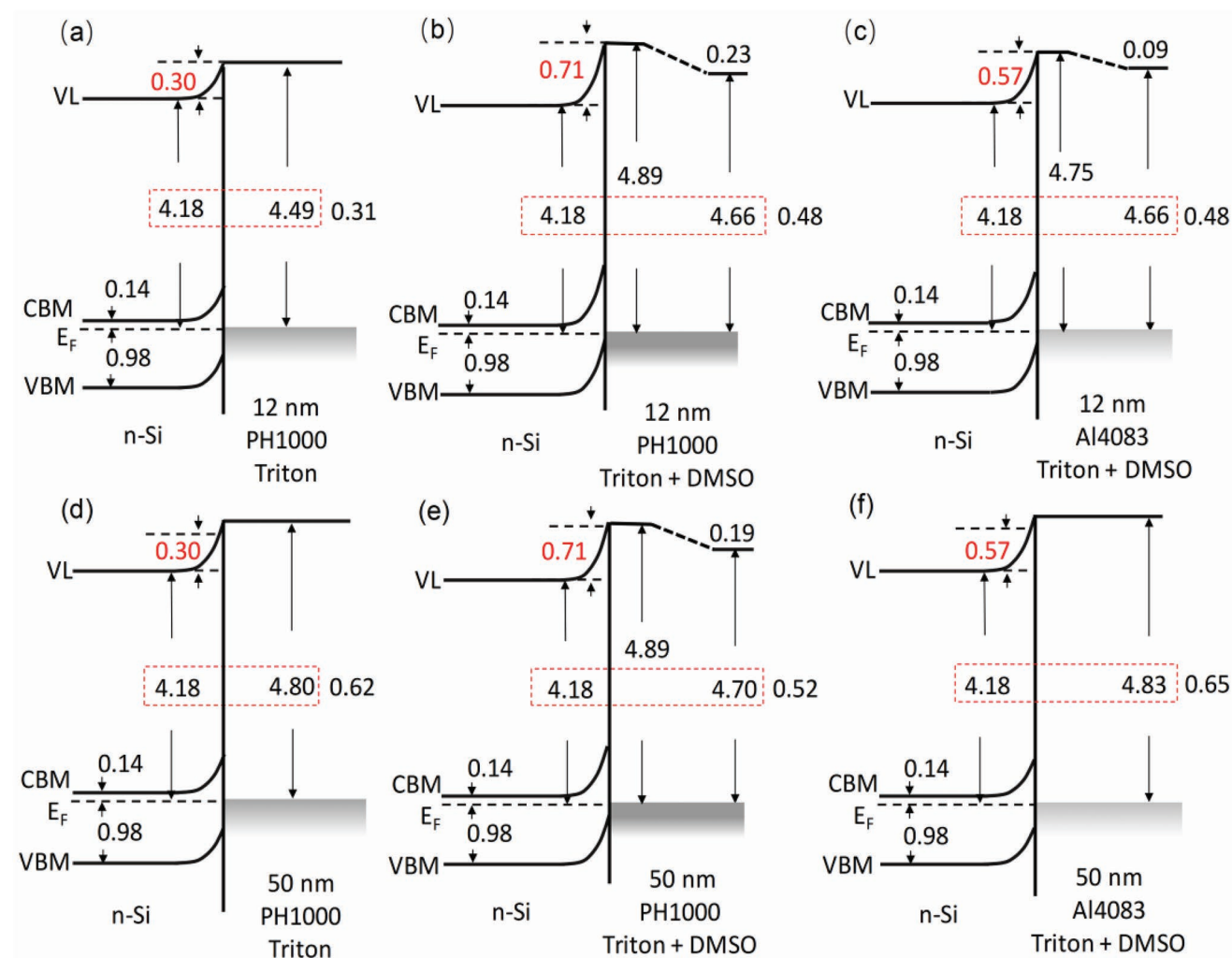


Figure 7. Experimentally obtained energy level diagrams of PEDOT:PSS/n-Si contacts. The room temperature bandgap of Si (1.12 eV) is taken from literature.^[23] All other values are based on the XPS and UPS results of this work (also summarized in Table 1). In each case, the lower limit of the band bending is taken from the Si 2p core level shift (Δ_{BE}). The WF shift (Δ_{WF}) is taken from UPS measurements. Dotted lines in the vacuum level (VL) indicate that the exact shape of the electrostatic potential energy within the PEDOT:PSS layer cannot be assessed experimentally (for details see the text). All values are in units of eV.

Table 4. PEDOT:PSS fabrication and thickness parameters on n-Si, except for sample 10 (bare native SiO₂ on n-Si).

Sample	Thickness [nm]	Solution	Spin-coating condition
S1	5(±2)	PH1000 (1 wt% Triton and 5 wt% DMSO): H ₂ O = 1:1.5 (mL:mL)	8500 rpm/60 s
S2	7(±2)	PH1000 (1 wt% Triton and 5 wt% DMSO): H ₂ O = 1:1.5 (mL:mL)	8000 rpm/60 s
S3	9(±2)	PH1000 (1 wt% Triton and 5 wt% DMSO): H ₂ O = 1:1 (mL:mL)	8500 rpm/60 s
S4	12(±2)	PH1000 (1 wt% Triton and 5 wt% DMSO): H ₂ O = 1:1 (mL:mL)	8000 rpm/60 s
S5	50(±3)	PH1000 (1 wt% Triton and 5 wt% DMSO)	4000 rpm/60 s
S6	12(±3)	PH1000 (1 wt% Triton): H ₂ O = 1:1 (mL:mL)	8000 rpm/60 s
S7	50(±5)	PH1000 (1 wt% Triton)	4000 rpm/60 s
S8	12(±2)	Al4083 (1 wt% Triton and 5 wt% DMSO): H ₂ O = 1:1.5 (mL:mL)	8500 rpm/60 s
S9	50(±3)	Al4083 (1 wt% Triton and 5 wt% DMSO)	4000 rpm/60 s
S10	12(±2)	PH1000: H ₂ O = 1:1.5 (mL:mL)	8000 rpm/60 s

Photoelectron Spectroscopy Measurements: XPS (Al K α , 1486.7 eV) and UPS (He I α , 21.22 eV) measurements were carried out in a SPECS photoelectron spectroscopy system, including an analysis chamber (base pressure: 2×10^{-10} mbar), an evaporation chamber (base pressure: 2×10^{-10} mbar), and a sample load-lock.^[42] All measurements were performed at room temperature (295 K). XPS and UPS spectra are plotted with respect to the Fermi level (E_F). The SECO spectra are plotted as function of kinetic energy corrected by the applied bias voltage (−3 V) and the analyzer WF. Thus, the SECO position corresponds to the position of the vacuum level above E_F , which is also referred to as WF. To compare the element atomic ratio from XPS, the spectra were fitted with a Shirley background and Voigt peaks. The peak areas were divided by the respective relative sensitivity factors.^[43] For the fitting of Si 2p and S 2p, the energy differences between Si 2p_{1/2}/Si 2p_{3/2} and S 2p_{1/2}/S 2p_{3/2} components were fixed at 0.60 and 1.20 eV, respectively, and the peak area ratio for both cases was fixed at 1:2.^[2b,6b]

Solar Cell Fabrication and Characterization: For n-Si/PEDOT:PSS solar cells the PEDOT:PSS layers were spin-coated at 4000 rpm for 60 s and annealed at 125 °C for 20 min. For n-Si/MoO_x solar cells, 25 nm MoO_x were thermally evaporated on n-Si. Finally, 200 nm thick Ag grid front electrodes with a finger width of 100 μ m and 200 nm thick Al rear electrodes were deposited by thermal evaporation (NANO 36, Kurt J. Lesker), respectively. The solar cells were characterized by a Newport solar simulator with air mass (AM) 1.5 G conditions at an illumination intensity of 100 mW cm^{−2}.

Supporting Information

Supporting Information is available from the Wiley Online Library or from the author.

Acknowledgements

Financial support from the National Key R&D Program of China (Grant No. 2017YFA0205002), the National Natural Science Foundation of China (Grant No. 91833303), the 111 Project of the Chinese State Administration of Foreign Experts Affairs, the Collaborative Innovation Center of Suzhou Nano Science and Technology (NANO-CIC), and the Deutsche Forschungsgemeinschaft (DFG)—Projektnummer 182087777—SFB 951 is gratefully acknowledged.

Conflict of Interest

The authors declare no conflict of interest.

Keywords

band bending, core level shifts, energy level alignment, inversion layer, PEDOT:PSS/Si solar cell

Received: April 30, 2019
Revised: August 19, 2019
Published online: October 30, 2019

- [1] a) J. He, P. Gao, Z. Yang, J. Yu, W. Yu, Y. Zhang, J. Sheng, J. Ye, J. C. Amine, Y. Cui, *Adv. Mater.* **2017**, 29, 1606321; b) H. Tong, Z. Yang, X. Wang, Z. Liu, Z. Chen, X. Ke, M. Sui, J. Tang, T. Yu, Z. Ge, Y. Zeng, P. Gao, J. Ye, *Adv. Energy Mater.* **2018**, 8, 1702921; c) E. L. Williams, G. E. Jabbour, Q. Wang, S. E. Shaheen, D. S. Ginley, E. A. Schiff, *Appl. Phys. Lett.* **2005**, 87, 223504; d) R. W. MacQueen, M. Liebhauer, J. Niederhausen, M. Mews, C. Gersmann, S. Jäckle, K. Jäger, M. J. Y. Tayebjee, T. W. Schmidt, B. Rech, K. Lips, *Mater. Horiz.* **2018**, 5, 1065.
- [2] a) M. Pietsch, S. Jäckle, S. Christiansen, *Appl. Phys. A* **2014**, 115, 1109; b) M. Pietsch, M. Y. Bashouti, S. Christiansen, *J. Phys. Chem. C* **2013**, 117, 9049.
- [3] P. Gao, Z. Yang, J. He, J. Yu, P. Liu, J. Zhu, Z. Ge, J. Ye, *Adv. Sci.* **2018**, 5, 1700547.
- [4] a) Z. Yang, P. Gao, J. He, W. Chen, W.-Y. Yin, Y. Zeng, W. Guo, J. Ye, Y. Cui, *ACS Energy Lett.* **2017**, 2, 556; b) H. Shi, C. Liu, Q. Jiang, J. Xu, *Adv. Electron. Mater.* **2015**, 1, 1500017.
- [5] a) N. Ikeda, T. Koganezawa, D. Kajiya, K.-i. Saitow, *J. Phys. Chem. C* **2016**, 120, 19043; b) J. P. Thomas, L. Zhao, D. McGillivray, K. T. Leung, *J. Mater. Chem. A* **2014**, 2, 2383.
- [6] a) Y. H. Nam, J. W. Song, M. J. Park, A. Sami, J. H. Lee, *Nanotechnology* **2017**, 28, 155402; b) S. Wu, W. Cui, N. Aghdassi, T. Song, S. Duhm, S.-T. Lee, B. Sun, *Adv. Funct. Mater.* **2016**, 26, 5035.
- [7] a) Z. Xia, P. Gao, T. Sun, H. Wu, Y. Tan, T. Song, S. T. Lee, B. Sun, *ACS Appl. Mater. Interfaces* **2018**, 10, 13767; b) Y. Liu, Z. G. Zhang, Z. Xia, J. Zhang, Y. Liu, F. Liang, Y. Li, T. Song, X. Yu, S. T. Lee, B. Sun, *ACS Nano* **2016**, 10, 704; c) J. He, P. Gao, Z. Ling, L. Ding, Z. Yang, J. Ye, Y. Cui, *ACS Nano* **2016**, 10, 11525.
- [8] a) J. Bullock, Y. Wan, Z. Xu, S. Essig, M. Hettick, H. Wang, W. Ji, M. Boccard, A. Cuevas, C. Ballif, A. Javey, *ACS Energy Lett.* **2018**, 3, 508; b) K. Yoshikawa, H. Kawasaki, W. Yoshida, T. Irie, K. Konishi, K. Nakano, T. Uto, D. Adachi, M. Kanematsu, H. Uzu, K. Yamamoto, *Nat. Energy* **2017**, 2, 17032.
- [9] a) O. Bubnova, Z. U. Khan, H. Wang, S. Braun, D. R. Evans, M. Fabretto, P. Hojati-Talemi, D. Dagnelund, J. B. Arlin, Y. H. Geerts, S. Desbief, D. W. Breiby, J. W. Andreasen, R. Lazzaroni, W. M. Chen,

- I. Zozoulenko, M. Fahlman, P. J. Murphy, M. Berggren, X. Crispin, *Nat. Mater.* **2014**, *13*, 190; b) Y. Xia, K. Sun, J. Ouyang, *Adv. Mater.* **2012**, *24*, 2436; c) X. Crispin, S. Marciniak, W. Osikowicz, G. Zotti, A. W. D. V. D. Gon, M. Fahlman, L. Groenendaal, F. D. Schryver, W. R. Salaneck, *J. Polym. Sci., Part B: Polym. Phys.* **2003**, *41*, 2561; d) J. Chen, Y. Shen, J. Guo, B. Chen, J. Fan, F. Li, B. Liu, H. Liu, Y. Xu, Y. Mai, *Electrochim. Acta* **2017**, *247*, 826; e) I. Lee, G. W. Kim, M. Yang, T. S. Kim, *ACS Appl. Mater. Interfaces* **2016**, *8*, 302.
- [10] a) N. Koch, A. Vollmer, A. Elschner, *Appl. Phys. Lett.* **2007**, *90*, 043512; b) M. A. Triana, H. Chen, D. Zhang, R. J. Camargo, T. Zhai, S. Duhm, Y. Dong, *J. Mater. Chem. C* **2018**, *6*, 7487.
- [11] A. S. Erickson, A. Zohar, D. Cahen, *Adv. Energy Mater.* **2014**, *4*, 1301724.
- [12] a) E. J. Bae, Y. H. Kang, K. S. Jang, S. Y. Cho, *Sci. Rep.* **2016**, *6*, 18805; b) Q. Liu, R. Ishikawa, S. Funada, T. Ohki, K. Ueno, H. Shirai, *Adv. Energy Mater.* **2015**, *5*, 1500744; c) J. P. Thomas, K. T. Leung, *Adv. Funct. Mater.* **2014**, *24*, 4978.
- [13] a) X. Shen, L. Chen, J. Pan, Y. Hu, S. Li, J. Zhao, *Nanoscale Res. Lett.* **2016**, *11*, 532; b) S. Jäckle, M. Mattiza, M. Liebhaber, G. Bronstrup, M. Rommel, K. Lips, S. Christiansen, *Sci. Rep.* **2015**, *5*, 13008.
- [14] a) S. Jäckle, M. Liebhaber, C. Gersmann, M. Mews, K. Jäger, S. Christiansen, K. Lips, *Sci. Rep.* **2017**, *7*, 2170; b) Q. Fan, Q. Zhang, W. Zhou, X. Xia, F. Yang, N. Zhang, S. Xiao, K. Li, X. Gu, Z. Xiao, H. Chen, Y. Wang, H. Liu, W. Zhou, S. Xie, *Nano Energy* **2017**, *33*, 436.
- [15] T. Sun, R. Wang, R. Liu, C. Wu, Y. Zhong, Y. Liu, Y. Wang, Y. Han, Z. Xia, Y. Zou, T. Song, N. Koch, S. Duhm, B. Sun, *Phys. Status Solidi—Rapid Res. Lett.* **2017**, *11*, 1700107.
- [16] M. Kröger, S. Hamwi, J. Meyer, T. Riedl, W. Kowalsky, A. Kahn, *Appl. Phys. Lett.* **2009**, *95*, 123301.
- [17] a) S. Jäckle, M. Liebhaber, J. Niederhausen, M. Buchele, R. Felix, R. G. Wilks, M. Bar, K. Lips, S. Christiansen, *ACS Appl. Mater. Interfaces* **2016**, *8*, 8841; b) P. Yu, C.-Y. Tsai, J.-K. Chang, C.-C. Lai, P.-H. Chen, Y.-C. Lai, P.-T. Tsai, M.-C. Li, H.-T. Pan, Y.-Y. Huang, C.-I. Wu, Y.-L. Chueh, S.-W. Chen, C.-H. Du, S.-F. Horng, H.-F. Meng, *ACS Nano* **2013**, *7*, 10780.
- [18] a) M. P. Seah, W. A. Dench, *Surf. Interface Anal.* **1979**, *1*, 2; b) B. Philippe, T. J. Jacobsson, J.-P. Correa-Baena, N. K. Jena, A. Banerjee, S. Chakraborty, U. B. Cappel, R. Ahuja, A. Hagfeldt, M. Odelius, H. Rensmo, *J. Phys. Chem. C* **2017**, *121*, 26655.
- [19] S. Tanuma, C. J. Powell, D. R. Penn, *Surf. Interface Anal.* **2005**, *37*, 1.
- [20] D. B. Hall, P. Underhill, J. M. Torkelson, *Polym. Eng. Sci.* **1998**, *38*, 2039.
- [21] a) J. Luo, D. Billep, T. Waechtler, T. Otto, M. Toader, O. Gordan, E. Sheremet, J. Martin, M. Hietschold, D. R. T. Zahn, T. Gessner, *J. Mater. Chem. A* **2013**, *1*, 7576; b) J. Y. Kim, J. H. Jung, J. J. D. E. Lee, *Synth. Met.* **2002**, *126*, 311.
- [22] Z. Zou, W. Liu, D. Wang, Z. Liu, E. Jiang, S. Wu, J. Zhu, W. Guo, J. Sheng, J. Ye, *Sol. Energy Mater. Sol. Cells* **2018**, *185*, 218.
- [23] S. Hu, M. H. Richter, M. F. Lichterman, J. Beardslee, T. Mayer, B. S. Brunschwig, N. S. Lewis, *J. Phys. Chem. C* **2016**, *120*, 3117.
- [24] S. Avasthi, S. Lee, Y. L. Loo, J. C. Sturm, *Adv. Mater.* **2011**, *23*, 5762.
- [25] H. Wang, S. V. Levchenko, T. Schultz, N. Koch, M. Scheffler, M. Rossi, *Adv. Electron. Mater.* **2019**, 1800891.
- [26] N. Koch, A. Vollmer, *Appl. Phys. Lett.* **2006**, *89*, 162107.
- [27] S. Fabiano, S. Braun, X. Liu, E. Weverberghs, P. Gerbaux, B. S. Brunschwig, M. Berggren, X. Crispin, *Adv. Mater.* **2014**, *26*, 6000.
- [28] O. Bubnova, Z. U. Khan, A. Malti, S. Braun, M. Fahlman, M. Berggren, X. Crispin, *Nat. Mater.* **2011**, *10*, 429.
- [29] S.-I. Na, G. Wang, S.-S. Kim, T.-W. Kim, S.-H. Oh, B.-K. Yu, T. Lee, D.-Y. Kim, *J. Mater. Chem.* **2009**, *19*, 9045.
- [30] Y. Liu, J. Zhang, H. Wu, W. Cui, R. Wang, K. Ding, S.-T. Lee, B. Sun, *Nano Energy* **2017**, *34*, 257.
- [31] X. Crispin, F. L. E. Jakobsson, A. Crispin, P. C. M. Grim, P. Andersson, A. Volodin, C. v. Haesendonck, M. V. d. Auwerar, W. R. Salaneck, M. Berggren, *Chem. Mater.* **2006**, *18*, 4354.
- [32] M. R. Lenze, N. M. Kronenberg, F. Würthner, K. Meerholz, *Org. Electron.* **2015**, *21*, 171.
- [33] a) I. Lange, J. C. Blakesley, J. Frisch, A. Vollmer, N. Koch, D. Neher, *Phys. Rev. Lett.* **2011**, *106*, 216402; b) T. Schultz, P. Amsalem, N. B. Kotadiya, T. Lenz, P. W. M. Blom, N. Koch, *Phys. Status Solidi (b)* **2019**, *256*, 1800299; c) T. Schultz, T. Lenz, N. Kotadiya, G. Heimel, G. Glasser, R. Berger, P. W. M. Blom, P. Amsalem, D. M. de Leeuw, N. Koch, *Adv. Mater. Interfaces* **2017**, *4*, 1700324.
- [34] M. Grundner, H. Jacob, *Appl. Phys. A Solids Surf.* **1986**, *39*, 73.
- [35] S.-S. Yoon, D.-Y. Khang, *Adv. Energy Mater.* **2018**, *8*, 1702655.
- [36] a) S.-S. Yoon, D.-Y. Khang, *J. Phys. Chem. Solids* **2019**, *129*, 128; b) A. T. M. Saiful Islam, R. Ishikawa, H. Shirai, in *Advanced Nanomaterials for Solar Cells and Light Emitting Diodes* (Ed: F. Gao), Elsevier, New York, **2019**, Ch. 4.
- [37] a) D. Zielke, C. Niehaves, W. Lövenich, A. Elschner, M. Hörteis, J. Schmidt, *Energy Proc.* **2015**, *77*, 331; b) M. U. Halbach, D. Zielke, R. Gogolin, R. Sauer-Stieglitz, W. Lövenich, J. Schmidt, *Sci. Rep.* **2019**, *9*, 9775.
- [38] A. B. Prakoso, Rusli, Z. Li, C. Lu, C. Jiang, *Semicond. Sci. Technol.* **2018**, *33*, 035016.
- [39] S. M. Sze, K. K. Ng, *Physics of Semiconductor Devices*, John Wiley & Sons, Hoboken, NJ, USA **2007**.
- [40] K. Fu, R. Wang, T. Katase, H. Ohta, N. Koch, S. Duhm, *ACS Appl. Mater. Interfaces* **2018**, *10*, 10552.
- [41] J. K. Tan, R. Q. Png, C. Zhao, P. K. H. Ho, *Nat. Commun.* **2018**, *9*, 3269.
- [42] M.-C. Lu, R.-B. Wang, A. Yang, S. Duhm, *J. Phys.: Condens. Matter* **2016**, *28*, 094005.
- [43] C. D. Wagner, L. E. Davis, M. V. Zeller, J. A. Taylor, R. H. Raymond, L. H. Gale, *Surf. Interface Anal.* **1981**, *3*, 211.